Understanding the exposure of marine life to electromagnetic fields generated by subsea cables

V. Caradonna, P. Sigray, A. B. Gill, A. Azzellino, D. Vicinanza and J. F. Borsani

Abstract— **Electromagnetic fields (EMF) generated by wave and tidal energy subsea power cables can potentially impact marine life. The primary source of artificial EMF is subsea power cables, whose estimates of the propagating levels are typically conducted using theoretical models. However, these models must be validated with empirical data collected *in situ*. This study proposes a new measurement methodology that enhances the accuracy of the estimated fields in the water column. The new methodology employs two fluxgate magnetometers operating simultaneously: one stationary near the cable and the other moved around to map spatial variations. The stationary magnetometer thus serves as a reference. Changes in the magnetic field recorded by the stationary fluxgate can be attributed solely to variations in the electric current flowing through the cable. The advantage of this configuration is that it enables linear corrections of changes in the cable current during measurement. Consequently, data from the moving fluxgate can be adjusted according to the fluctuating current. This methodology will produce corrected data suitable for modelling where the current is assumed to be constant. The methodology was tested *in situ* on a High Voltage Alternating Current offshore wind export cable. Additionally, it was observed that there were two contributions to the observed magnetic field: the magnetic field from a balanced load that attenuates effectively with increasing distance and the magnetic field generated by an unbalanced load that decreases more slowly and, as a result, influences a larger volume.**

Keywords— **balanced current, data collection, EMF propagation, magnetic field, subsea power cables, unbalanced current.**

Part of a special issue for EWTEC 2025. Original version published in EWTEC 2025 proceedings at doi.org/10.36688/ewtec-2025-720.

This publication is produced with the support of a scholarship grant co-financed by DM 118/23 PNRR (M4C1 – Inv. 4.1 PNRR).

V. Caradonna is with the University of Campania Luigi Vanvitelli, Department of Engineering Via Roma 29, 81031 Aversa, Italy and with ISPRA, Via Vitaliano Brancati 48, 00144 Roma, Italy (e-mail: valentina.caradonna@unicampania.it).

P. Sigray is with KTH Royal Institute of Technology, Department of Engineering Mechanics /Marine Engineering/ Sensing & Environment, Teknikringen 8, plan 4, SE - 100 44 Stockholm, Sweden (e-mail: sigray@kth.se).

A. B. Gill was with Centre for Environment, Fisheries and Aquaculture Science, Pakefield Road, Lowestoft, Suffolk, NR33 0HT, U.K. He is now with Australian Institute of Marine Science, Indian Ocean Marine Research Centre, Crawley WA 6009, Australia (email: a.gill@aims.gov.au).

A. Azzellino is with the Civil and Environmental Engineering Department of the Politecnico di Milano, P.za Leonardo da Vinci, 32, 20133 Milan, Italy (e-mail: arianna.azzellino@polimi.it).

D. Vicinanza is with the University of Campania Luigi Vanvitelli, Department of Engineering Via Roma 29, 81031 Aversa, Italy (e-mail: diego.vicinanza@unicampania.it).

J. F. Borsani is with ISPRA, Via Vitaliano Brancati 48, 00144 Roma, Italy (e-mail: jf.borsani@gmail.com).

Digital Object Identifier: https://doi.org/10.36688/imej.9.39-46

I. Introduction

Wave and tidal energies are important resources for the decarbonization process. However, their use raises environmental concerns, including electromagnetic field (EMF) emissions into the marine environment. Subsea power cables are the primary source of artificial EMF at sea [1]. In the case of wave and tidal devices, there may be additional sources of EMF, such as permanent magnets mounted on certain turbines [2]. A network of cables between devices, known as inter-array cables, connects all devices either to a collector device or an offshore substation. Current is then carried to the onshore grid through several high-voltage export cables. The transmission of marine derived power generates EMF in the adjacent environment, namely the water column and seabed [1], [3]. The electrical current in the cables induces magnetic fields (expressed as B-field; measured in μT). In cables transmitting alternating currents (AC) changing magnetic fields also create induced electric fields (i-E field). In the ocean, this leads to electric currents flowing through the saline water [2], [4]. AC and DC (Direct Current) are the two types of transmission used for marine renewable energy devices. These can vary in voltage—low, medium, or high (HV)—with HVAC being the most common for distances up to 50 km from the shore and HVDC the most suitable for further distances from the shore [5], [6]. Cables are typically buried within the seabed but may be placed on top with external protection when the seabed is rocky. They can also be deployed in the water column for floating devices, such as wave converters [5], [7].

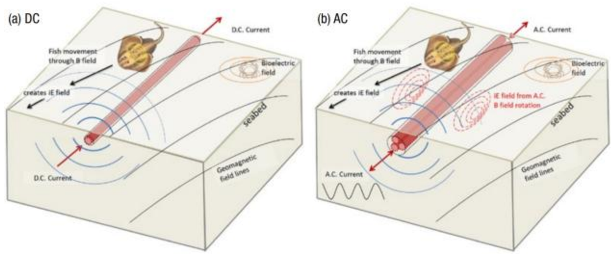

Fig. 1. Representation of the magnetic field, electric field (E-field) and induced electric field in the case of DC cables (a) and AC cables (b) experienced by a sensitive species [4].

All species live within an EM-environment and several have been determined as sensitive to electromagnetic fields (Fig. 1). They include chondrichthyes (e.g. sharks and rays), crustaceans (e.g. lobsters), certain teleosts (e.g. salmonids), as well as chelonians (i.e. sea turtles), and cetaceans (i.e. whales and dolphins) [8], [9]. Electromagnetic sense can be used for prey detection as well as orientation and communication [8], [9]. EMF radiated by renewable energy devices is likely to disturb some of these fundamental functions [10]. Effects of exposure to anthropogenic EMF were reviewed by [11] as well as [12]. Observed effects include behavioural changes in foraging as well as swimming and sheltering (e.g. [13], [14]). Subtle modifications in migration routes and swimming speed were also noted, e.g. by [15] and [16]. Other observations are attraction or repulsion towards EMF sources, alterations in early-stage development, as well as freeze response activation (e. g. [17], [18], [19]). Further studies reported no significant response by examined species when submitted to an artificial magnetic field, e.g. [20].

While the above suggests an effect, more substantial evidence on how sensitive species perceive anthropogenic EMF is necessary, as emphasized by [21]. To achieve this objective, the first step is to understand the EMF propagation of subsea cables. Typically, modelling is employed to simulate the EMF environment that animals are likely to encounter [21]. Discrepancies between *in situ* measurements and modelling underscore the importance of comparing models with measurement results for a reliable understanding of EMF [22]. Section II addresses the challenges in measuring magnetic fields. The new methodology is detailed in Section III. Section IV presents findings from a simulated case study where a sudden drop in power transmission occurs. In Section V, the methodology is applied, and the results from an *in situ* measurement are analysed, considering both balanced and unbalanced loads. Finally, conclusions are drawn.

II. B-FIELD MEASUREMENTS AND OBSTACLES

Until today, few *in situ* measurements have been conducted to describe the EMF of subsea cables [11]. Such endeavours were made employing autonomous underwater vehicles (AUVs) or vessel-towed three-axis sensors. The magnetic field, and sometimes the electric field, were measured simultaneously at various distances from the cable. The sensor was moved across the cable approximately perpendicular [23], [24], [25], [26], [27]. Previous observations from [28] indicate that this methodology may have limitations. Throughout a measurement session, the intensity of the current flowing through the cable is likely to change. If this occurs, the resulting B-field levels may show unusual changes due to temporal increases or decreases in current (Fig. 4 blue line). A concerning consequence is that data collected using this procedure does not solely represent B-field values as a function of distance; they also depend on the current flowing through the cable. If the cables were consistently powered at the same level, methods to compensate for potential changes in current would not be necessary. However, experience shows that changes in current during *in situ* measurements are likely to occur. Knowing the power data corresponding to the time of data acquisition could offer a solution to this issue. Unfortunately, researchers do not always have access to this type of “commercial” data. Even when power data are provided, their time resolution is generally low, which is not ideal for data adjustment procedures. Therefore, alternatives must be explored. In this paper we present a new approach. The methodology was tested for magnetic field data collection; nevertheless, the procedure is also valid for the electric field.

III. METHODOLOGY

Data were collected at the landfall zone of a 220kV HVAC offshore wind export cable in northern U.K. in early November 2024, from 09:48 to 10:28 am. For practical reasons, the measurements were conducted on land where the cables came approximately within 1.5 m burial depth parallel to the surface after being horizontally directionally drilled under the nearby beach. Knowing the exact value of the burial depth is not necessary in this paper, since the aim is not modelling the emitted magnetic field. Measuring the magnetic field on land does not limit the validity of the results, as EMF propagation was quasi-static, meaning the difference in magnetic field propagation between water and land can be ignored. It is possible to acquire data underwater, but of course it would be more complicated. One crucial aspect is that the sensors must remain stationary during data collection, hence, measurements were conducted on land to achieve greater stability than in water. The cable was a 3-core 220kV HVAC cable with three copper conductors. The conductors are helically twisted to reduce the emitted magnetic field compared to the untwisted configuration [28], [29], [30]. Although the cable connects to an offshore wind farm, our proposed methodology is equally applicable to wave and tidal energy converters. The rationale behind our methodology remains relevant across cables for different devices.

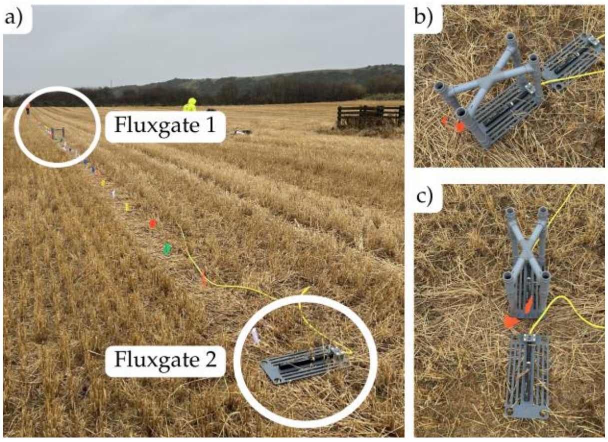

Fig. 2. Field setup with positions of the two fluxgates along a survey transect during data collection. a) upper left: fluxgate 1 (stationary on the cable); bottom right: fluxgate 2 (moving); b) and c) both fluxgates at *point zero* in two different configurations: b) fluxgate 2 behind fluxgate1; c) fluxgate 2 in front of fluxgate 1.

A digital EMF meter (EMF-390), which is a portable device able to identify an EMF source, was used to determine the location of the cable. The meter was held in hand and moved along the expected perpendicular direction to the cable direction until maximum magnetic field intensity was obtained. This location was assumed to be vertically above the cable. The position was marked with a flag and named *point zero*. Then, flags were placed perpendicularly to the expected cable direction at every metre on both the east and west sides, extending up to 20 meters from *point zero* (Fig. 2).

Two three-axis fluxgate magnetometers (Bartington Mag-13MSS1000) were utilized for data collection. They were connected via separate cables to a data acquisition unit (Bartington Spectramag 6), which in turn was connected to a laptop for data acquisition and real-time visualization. The fluxgates were oriented parallel to the power cable, all aligned with one another, with the output cables facing the landside. Fluxgate 1 (also fl_1) remained stationary at the *point zero* throughout the entire data collection period. Consequently, any recorded changes in the B-field can only be attributed to variations in the current flowing through the cable, as the distance from the cable was constant. Fluxgate 1 served as the B-field reference. Fluxgate 2 (also fl_2) was moved one metre at a turn, perpendicular to the cable, as shown in Fig. 2a. This fluxgate had the role to measure the B-field as a function of distance from the cable. The range extended from -20 m (20 m away from the cable toward the east side) to +20 m (20 m away from the cable toward the west side).

The two fluxgates were sampled synchronously. Measurements were collected for 30 seconds at each flag, with a sample rate of 1 kHz. This resulted in a total of 30000 samples at each position. When both fluxgates were at *point zero*, data were collected in two different configurations. Fluxgate 2 was placed once behind fluxgate 1 (Fig. 2b) and once in front of the latter (Fig. 2c).

TABLE I
B-FIELD MEAN VALUES AND LINEAR FITTINGS

fl_2 d_{oi} (m)	B_{tot} fl_{1i} (μT)	B_{tot} fl_{2i} (μT)	Linear fittings $fl_1 - fl_2$	R^2
-20	5.197	0.094	y=0.019x-0.003	0.333
-19	5.035	0.098	y=0.042x-0.115	0.289
-18	5.020	0.098	y=-0.004x+0.119	0.004
-17	4.803	0.100	y=0.061x-0.192	0.311
-16	4.749	0.100	y=0.014x+0.036	0.274
-15	4.696	0.103	y=0.037x-0.071	0.417
-14	4.611	0.105	y=-0.024x+0.214	0.066
-13	4.629	0.117	y=-0.148x+0.804	0.128
-12	4.686	0.120	y=0.024x+0.008	0.452
-11	4.684	0.132	y=0.025x+0.017	0.044
-10	4.666	0.140	y=0.037x-0.036	0.473
-9	4.547	0.150	y=0.030x+0.013	0.580
-8	4.551	0.171	y=0.034x+0.018	0.698
-7	4.479	0.199	y=0.038x+0.029	0.291
-6	4.535	0.244	y=0.095x-0.185	0.783
-5	4.725	0.344	y=0.077x-0.017	0.459
-4	4.771	0.508	y=0.092x+0.071	0.651
-3	4.830	0.855	y=0.183x-0.030	0.973
-2	4.799	1.529	y=0.312x+0.034	0.942
-1	4.820	3.081	y=0.699x-0.288	0.993
0	4.863	4.863	y=0.826x-0.082	0.988
+1	4.902	5.043	y=1.031x-0.010	0.999
+2	5.223	2.957	y=0.511x+0.290	0.938
+3	5.230	1.367	y=0.261x+0.001	0.978
+4	5.305	0.677	y=0.171x-0.229	0.889
+5	5.116	0.365	y=0.423x-1.80	0.375
+6	5.188	0.234	y=0.060x-0.077	0.480
+7	5.172	0.179	y=0.024x+0.054	0.766
+8	5.303	0.156	y=0.027x+0.014	0.335
+9	5.362	0.139	y=0.021x+0.027	0.752
+10	5.166	0.122	y=0.029x-0.028	0.597
+11	5.196	0.114	y=0.141x-0.617	0.032
+12	5.219	0.099	y=0.002x+0.089	0.003
+13	5.279	0.095	y=-0.155x+0.915	0.132
+14	5.167	0.080	y=0.011x+0.024	0.396
+15	5.248	0.075	y=-0.001x+0.083	0.002
+16	5.290	0.067	y=0.007x+0.031	0.046
+17	5.329	0.061	y=0.011x+0.001	0.217
+18	5.347	0.057	y=0.059x-0.256	0.235
+19	5.442	0.053	y=0.027x+0.201	0.150
+20	5.376	0.047	y=0.009x-0.002	0.072

Mean B-field is reported for fl_1 (fl_{1i}) as well as for fl_2 (fl_{2i}) for each 30 s measurement corresponding to the position i of fl_2 (i = -20 m, -19 m,…, +20 m). At 0 m fl_1 value is replicated for fl_2. This choice was made because fl_2 was not aligned with all measurements taken from -20 m to +20 m. To avoid biases during the data correction process, fl_1 value was directly used when using the mean method. Linear fittings of every pair fl_1-fl_2 and the corresponding R^2 are reported.

A. *Data analysis*

MATLAB version 24.1.0.2628055 (R2024a) Update 4 was used for data analysis. The magnetic field was acquired through its x (B_x), y (B_y), and z (B_z) components by both fluxgates. The influence of the Eart's magnetic field was removed by subtracting the mean of each component before the amplitude of the total magnetic field (hereafter magnetic field) was calculated according to the formula:

$$B_{tot} = \sqrt{{B_x}^2 + {B_y}^2 + {B_z}^2} \quad (1)$$

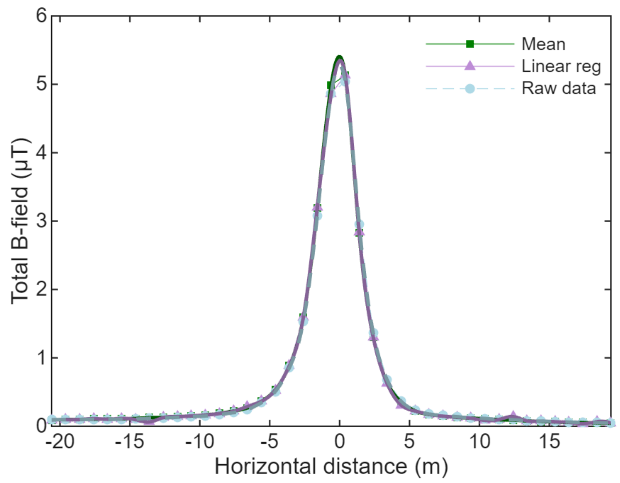

Fig. 3. Total B-field of fl_2 as a function of distance from the cable (d_1) in the case of data corrected with the mean method (green), data corrected with the linear regression method (violet), and raw data without any correction (light blue).

Hilbert transforms were used to determine the positive and negative envelopes of the magnetic components. This exercise was performed to assure that the observed change in B-field was due to changing magnetic field density and not to electronic drift. Two strategies were employed to adjust Fluxgate 2 data. The first involved the mean, whereas the second utilised the correlation between Fluxgate 1 and 2.

Concerning the first method, the mean B-field of each 30 second recording was determined for fl_1 (fl_{1_i}) as well as for fl_2 (fl_{2_i}), as listed in Table I. Index i is used to distinguish the different positions covered by fluxgate 2, i.e. each metre from -20 m to +20 m.

With respect to the 0 m position, two measurements per fluxgate exist due to the dual configuration of fluxgate 2 (Fig. 2b and 2c). Therefore, only one of the two configurations was chosen for the analysis.

Once the 30-second means (fl_{1i} and fl_{2i}) were computed, the overall mean of fl_{1i} was determined, denoted as $\overline{fl_1}$. This value represents the average of the previously 41 computed 30-second means. The overall mean $\overline{fl_1}$ was then used to adjust each measurement made by fl_2 at the position i, according to the following formula:

$$fl_2adj_i = fl_{2_i}\frac{\overline{fl_1}}{fl_{1_i}} \quad (2)$$

By averaging all fl_{1_i} values, $\overline{fl_1}$ turned out to be 4.989 μT.

An example of the application of (2) is provided. When Fluxgate 2 is at +19 m, mean B-field recorded by Fluxgate 1 is 5.442 μT, which is approximately 9% higher than $\overline{fl_1}$ (4.989 μT). Consequently, the corresponding value of fl_2 must be reduced to account for this variation. The initial value of fl_2 at +19 m is 0.053 μT (Table I). With the application of (2) the adjusted value of fl_2 becomes 0.049 μT. The small difference between the original and adjusted values is due to the relatively weak fluctuation detected by Fluxgate 1. In principle, the fundamental aspect of this methodology is that Fluxgate 1 allows 1) the detection of eventual changes in the current flowing into the cable and 2) the right compensation for these changes at different distances from the cable.

The second method was based on the hypothesis that there is a linear relationship between fl_1 and fl_2 at each position. A regression was performed for each measurement pair using linear regression (Table I). fl_1 was treated as the independent variable and fl_2 was the dependent one. Thus, fl_2 values were adjusted according to fl_1 using the regression. $\overline{fl_1}$ (4.989 μT) was again substituted to the x value at each distance of every equation to compare the two methods. The two strategies are strictly comparable, except for a few observations (Fig. 3).

The linear fitting method can be extremely useful for predictions at distances closer to the cable. For further distances R^2 becomes too low, and adjustments seem not to be reliable anymore (see Table I).

The data analysis revealed that the *point zero* was not situated directly above the cable, which will affect the comparison between measured and modelled data. Thus, the *point zero* was adjusted horizontally by 0.60 m using the following formula:

$$d_1 = d_o - 0.60 \quad (3)$$

Table I shows the original horizontal distance from the cable (d_o), while graphs of Fig. 3 and Fig. 4 are plotted using the corrected distances (d_1). Proof of this horizontal offset is the fact that, in Fig. 3 as well as in Fig. 4, when $d_1 = 0\,m$ there is no corresponding field observation marked with a symbol. This is because the curve had to be shifted to align its peak with the cable position, i.e. at 0 m. Fig. 3 and fig. 4 clearly show that field observations do not correspond exactly to each metre but are all horizontally displaced. All of this demonstrate that *point zero* was not placed exactly above the cable.

Whilst the curve describing the raw data does not appear very different from the two corrected modelled datasets (Fig. 3), the variation of the current measured by fl_1 was weak and the corresponding variation of fl_2 was low. In the next section, the result of a simulation across different currents emphasises why the method is important for understanding changes across a range of currents transmitted.

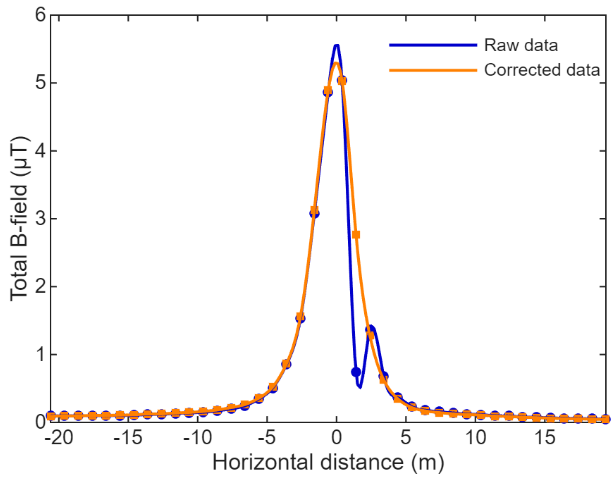

Fig. 4. B-field measured by fl_2 as a function of distance from the cable (d_1) in the case of raw data (blue) and data corrected with the mean method (orange).

IV. The Simulation

The simulation is used for the visualization of the method. It is assumed that the linear relationship still holds when the measured values are lower. The simulation was conducted using the original data. All recorded B-field values reported in Table I were kept unchanged. The only modified measurements were those acquired when fl_2 was at +2 m (meant as d_o here and hereafter). The B-field values of both fl_1 and fl_2 were reduced by 75% to simulate a significant drop in the current during data acquisition at that position. We compared the measurements obtained while fl_2 was at +2 m with those recorded when fl_2 was at +20 m because the time interval between the two data acquisitions was substantial, resulting in a high likelihood of a change in the current flowing into the cable, for the period we collected. Table II summarises the results for both fluxgates. We have to look at fl_1 values to understand the usefulness of having a stationary fluxgate. At 10:10 fl_2 was recording the B-field at +2 m from the cable. In the meantime, fl_1 was doing the same at *point zero*. The simulated mean value for fl_1 was 1.31 μT. Seventeen minutes later, fl_2 was relocated 20 m away from the *point zero*. At 10:27, fl_1 was measuring the B-field, and its mean value was 5.37 μT. The data indicate that the B-field changed significantly in 17 minutes at the *point zero* (5.37 μT vs. 1.31 μT). This illustrates the strength of our methodology.

Such imbalance at *point zero* can be corrected once it is noted. Purely for demonstration purposes, we wanted to show what happens if such data with the simulated value are adjusted. The mean method is used for the demo. Because of the 75% drop at +2 m, a new $\overline{fl_1}$ had to be determined before the application of (2). It resulted in 4.894 μT. B-field values reported in Table II were used for fl_1 and fl_2 when at the position *i* +2 m. Values reported in Table I were used for all the remaining positions for both fluxgates. The comparison between raw data and those adjusted with (2) is shown in Fig. 4. The blue line, i.e. the raw data, is characterized by a strong drop of the B-field at +2 m. Such drop corresponds to the simulated drop of the current at 10:10 am. The result is an asymmetrical curve. Using fl_1 data is possible to compensate for this imbalanced (orange curve). After the correction, B-field values are more accurate, and subsequent modelling will be more reliable. It should be stressed that the current drop was overemphasized in this simulation, just to show the strength of this methodology. Nevertheless, such variations in the current might occur in reality.

Table II
B-Field Comparison for fl_2 at +2 m and fl_2 at + 20 m

Time (am)	Position of $fl_2(d_o)$	Fluxgate	B-field
10:10	+2 m	1	1.306 μT
10:10	+2 m	2	0.739 μT
10:27	+20 m	1	5.376 μT
10:27	+20 m	2	0.047 μT

Comparison of the B-field of fl_1 while fl_2 was at +2 m (Time 10:10) and then at + 20 m (Time 10:27). B-field values are always expressed as average value of each 30 s-recording. Comparison is useful to understand that changes in the B-field, i.e. in the current flowing into the cable, are possible. Eventual changes must be taken into account when modelling B-field propagation.

V. Unbalanced Current

When dealing with three-phase power transmission, two important concepts must be defined: balanced and unbalanced systems. An ideal condition corresponds to a balanced system, in which phase currents are displaced from each other by 120 degrees, and the currents flowing through each phase have equal magnitude. In real situations we might encounter unbalanced systems. These arises when there is a disruption in current and/or phase, causing more current to flow through one particular phase to which the load is connected[1].

High voltage distribution lines are likely to exhibit a modest unbalanced current phenomenon [31]. Its occurrence was investigated herein in a descriptive manner. The presence of unbalanced current affects the propagation of the B-field. Theoretically, the B-field should attenuate significantly at a close distance to the cable when the system is dominated by a balanced load. The helical twist of the cable further enhances the attenuation [29]. If there is only a balanced load, sensitive species will encounter a magnetic field limited to the immediate vicinity of the cable. However, the B-field attenuation changes when the power transmission is

[1] https://www.theelectricalguy.in/tutorials/three-phase-balanced-vs-unbalanced-system-load/

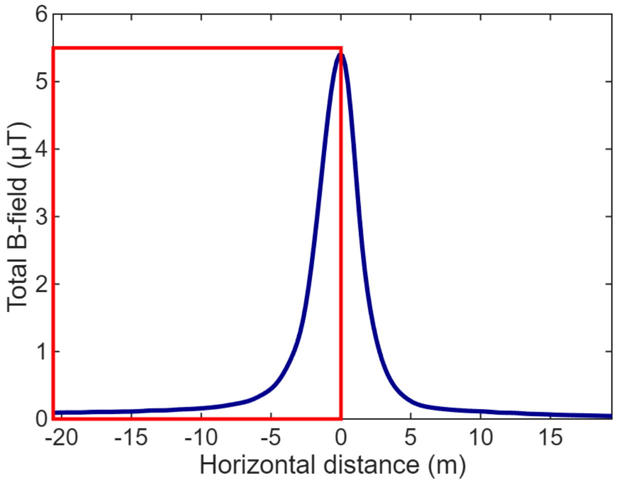

Fig. 5a. Total B-field of data corrected with the mean as a function of distance from the cable (d_1). For the next steps we consider only the left side (in red).

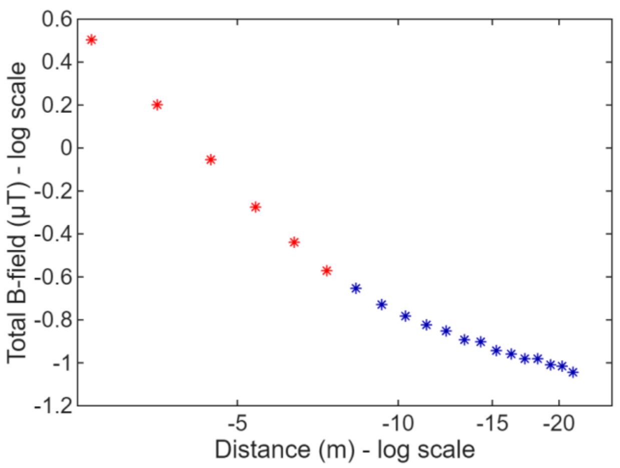

Fig. 5b. Total B-field on the logarithmic scale as a function of distance from the cable on the logarithmic scale (d_c). Dots with different colours indicate different linear fittings.

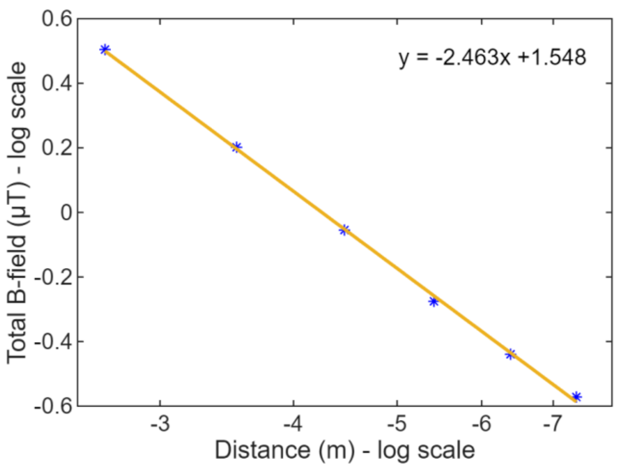

Fig. 5c. Linear relationship between the B-field and the distance from the cable in the near field of the cable (up to 7m).

unbalanced. At greater distances, the B-field will predominantly reflect the unbalanced current, even if it is much weaker than the balanced currents. At a certain distance, the unbalanced current will become the

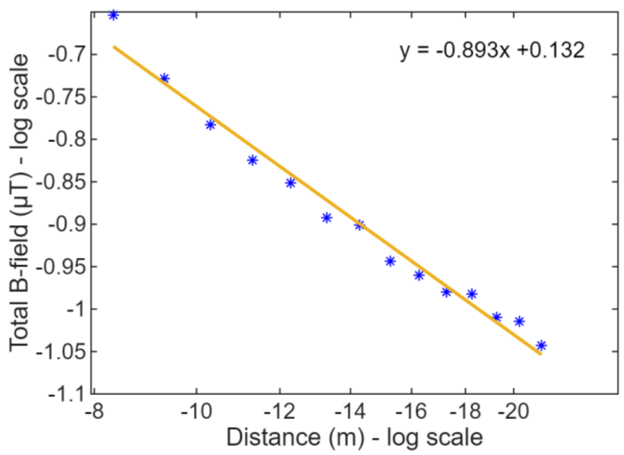

Fig. 5d. Linear relationship between the B-field and the distance from the cable when further from the latter (from 8 m to 20 m).

prevailing one since it does not nullify [32]. In this scenario, the magnetic field extent is greater in area. Therefore, species might be exposed over greater distances from the cable, up to tens of metres, as highlighted in [11]. Quantifying the unbalanced component is crucial for an accurate environmental impact assessment of marine renewable energy devices. Previous studies indicate that the unbalanced current decreases with distance according to the relation $1/r$, while the balanced component attenuates according to the relation $e^{-\frac{2\pi r}{p}} \cdot 1/r^2$, where the first factor is due to radial offset of the three conductors and the second due to the helical twist [22]. r is the radial distance measured from the centre of the cable to the measurement location, and p is the pitch of the helical twist (corresponds to lay length). The investigation of the unbalanced current was made using the data corrected applying the earlier described mean method. Only the left side of the curve is shown in Fig. 5a. The right side gave the same result.

Distances from the cable were corrected using (3) as well as adjusting for the offset inferred by the assumed burial depth (1.5 m):

$$d_c = \sqrt{{d_1}^2 + 1.5^2} \tag{4}$$

Distance and B-fields were converted to the logarithmic scale in base 10. It is clear that the result does not follow a straight line (Fig 5b). The data were split into two groups to restrict the fitting to “close” to and “far” from the cable. B-field values at a closer distance to the cable (up to 7 m) were described by the equation $y = -2.463x + 1.548$ $(R^2 = 0.999)$ (Fig 5c). For a further distance (from 8 m up to 20 m) B-values are defined by a different equation: $y = -0.8933x + 0.1322$ $(R^2 = 0.980)$ (Fig 5d).

There are two indications of the unbalanced current hypothesis. The first one is that the B-field is described as $1/r$, and the second is the variations still present in Fig. 5d after the corrections are made. The reason might be that the method in this study compensated for variations in the balanced load. Quantification of the unbalanced component should be an objective of future study to ensure EMF modelling is representative of the reality of the total EM-environment encountered by species.

VI. CONCLUSION AND FUTURE STEPS

The novelty and significance of our data collection method have been demonstrated, especially given the current lack of guidelines or regulations for EMF measurements and their related environmental impact assessment. This method is essential for obtaining a reliable dataset, particularly in *in situ* conditions, where large power variations are expected, due to typically weak winds (and consequently low wave heights) during field experiments.

The ultimate goal is to quantify the magnetic field exposure that could potentially impact marine species by employing models that align with the measurements. Developing a suitable model will be possible when accurate information on the measured cable as well as power data will be obtained. Unfortunately, at this stage the authors have not received them yet.

Existing models are applied considering only the balanced load. Our results enhance the characterisation of the balanced current and represent a step forward in comparing models with real data. Findings indicate that variations can be compensated by accounting for changes in the balanced load, as the stationary fluxgate—being close to the cable—is primarily influenced by it. However, our results highlight a new challenge. Beyond a distance of 6/7 metres, the magnetic field appears to be primarily influenced by unbalanced loads, which our current method cannot compensate for. A potential solution is to extend the method by incorporating a second stationary fluxgate positioned at a greater distance, allowing for a more comprehensive assessment.

We encourage the collection of EMF measurements from subsea cables in situ. At present, the EMF emitted by wave and tidal energy converters has not been investigated. The focus should be expanded to include cables connected to this type of energy generation.

With respect to the transmission operators, the unbalanced component cannot be ignored, even if it is much weaker compared to numbers encountered in high-power transmission systems. Its identification may help to set mitigation strategies, which may favour power transmission as well as a decrease of the area that might impact sensitive species.

ACKNOWLEDGEMENT

V. Caradonna thanks Peter Sigray for his support on EMF and Fabrizio Borsani for making the trip to Sweden possible.

The lead author wants also to thanks her supervisors Arianna and Diego for keeping her on track.

The authors are sincerely grateful to A. B. Gill and B. Kneafsey, Cefas for enabling the data collection. Thanks to the Crown Estate OWEC programme for funding the FLOWERS project to purchase the field equipment.

REFERENCES

[1] A. B. Gill, I. Gloyne-Philips, J. Kimber, and P. Sigray, "Marine renewable energy, electromagnetic (EM) fields and EM-sensitive animals," in *Marine Renewable Energy Technology and Environmental Interactions*, Springer, 2014, ch. 6, pp. 61–79. doi: 10.1007/978-94-017-8002-5_6.

[2] A. B. Gill, M. Bartlett, and F. Thomsen, "Potential interactions between diadromous fishes of U.K. conservation importance and the electromagnetic fields and subsea noise from marine renewable energy developments," *J. Fish Biol*., vol. 81, no. 2, pp. 664–695, Jul. 2012, doi: 10.1111/j.1095-8649.2012.03374.x.

[3] M. Slater, R. Jones, and A. Schultz, "The prediction of electromagnetic fields generated by submarine power cables," Report to Oregon Wave Energy Trust (OWET), 47 pp, 2010. [Online] Available: https://ir.library.oregonstate.edu/concern/technical_reports/h702q691k

[4] A. B. Gill, and M. Desender, "Risk to Animals from Electromagnetic Fields Emitted by Electric Cables and Marine Renewable Energy Devices," in *OES Environmental 2020 State of the Science Report: Environmental Effects of Marine Renewable Energy Development Around the World*. Report for Ocean Energy Systems (OES), pp. 86-103, Sep. 2020. doi: 10.2172/1633088.

[5] A. J. Collin, A. J. Nambiar, D. Bould, B. Whitby,M. A. Moonem, B. Schenkman, S. Atcitty, P. Chainho, A. E. Kiprakis, "Electrical Components for Marine Renewable Energy Arrays: A Techno-Economic Review," *Energies*, vol. 10, no. 12, Dec. 2017, doi: 10.3390/en10121973.

[6] E. P. P. Soares-Ramos, L. de Oliveira-Assis, R. Sarrias-Mena, and L. M. Fernández-Ramírez, "Current status and future trends of offshore wind power in Europe," *Energy*, vol. 202, Jul. 2020, doi: 10.1016/j.energy.2020.117787.

[7] S. H. Yang, J. W. Ringsberg, and E. Johnson, "Parametric study of the dynamic motions and mechanical characteristics of power cables for wave energy converters," *J. Mar. Sci. Technol.* vol. 23, no. 1, pp. 10–29, Mar. 2018, doi: 10.1007/s00773-017-0451-0.

[8] L. A. Wilkens, and M. H. Hofmann, "Behaviour of animals with passive, low-frequency electrosensory systems," in "*Electroreception*". New York, NY: Springer, 2005, ch. 2, pp. 229–263. [Online] Available: https://link.springer.com/chapter/10.1007/0-387-28275-0_9

[9] W. Wiltschko, and R. Wiltschko, "Magnetic orientation and magnetoreception in birds and other animals," *J. Comp. Physiol. A Neuroethol. Sens. Neural. Behav. Physiol*., vol 191, no. 8, pp 675-693, Aug. 2005. doi: 10.1007/s00359-005-0627-7.

[10] G. Boehlert and A. B. Gill, "Environmental and ecological effects of ocean renewable energy development: a current synthesis," *Oceanography*, vol. 23, no. 2, pp. 68–81, 2010, doi: https://doi.org/10.5670/oceanog.2010.46.

[11] Z. L. Hutchinson, D. H. Secor, and A. B. Gill, "The interaction between resource species and electromagnetic fields associated with electricity production by offshore wind farms," *Oceanography*, vol. 33, no. 4, pp. 96–107, 2020, doi: 10.5670/oceanog.2020.409.

[12] D. Nyqvist, C. Durif, M. G. Johnsen, K. De Jong, T. N. Forland, and L. D. Sivle, "Electric and magnetic senses in marine animals, and potential behavioral effects of electromagnetic surveys," *Mar. Environ. Res*., vol. 155, Mar. 2020, doi: 10.1016/j.marenvres.2020.104888.

[13] A. B. Gill et al., COWRIE 2.0 Electromagnetic Fields (EMF) Phase 2: EMF-sensitive fish response to EM emissions from sub-sea electricity cables of the type used by the offshore renewable energy industry. COWRIE Ltd., 2009. [Online] Available: https://tethys.pnnl.gov/sites/default/files/publications/Sensitive_Fish_Response_to_EM_Emissions_from_Offshore_Renewable.pdf

[14] K. Scott, P. Harsanyi, and A. R. Lyndon, "Understanding the effects of electromagnetic field emissions from Marine Renewable Energy Devices (MREDs) on the commercially important edible crab, Cancer pagurus (L.)," *Mar. Pollut. Bull.*, vol. 131, pp. 580–588, Jun. 2018, doi: 10.1016/j.marpolbul.2018.04.062.

[15] W. Westerberg and M. L. Begout-Anras, "Orientation of silver eel (Anguilla anguilla) in a disturbed geomagnetic field," *Advances in fish telemetry*, 149-158, 2000, pp. 149–158.

[16] M. T. Wyman et al., "Behavioral responses by migrating juvenile salmonids to a subsea high-voltage DC power cable," *Mar. Biol.*, vol. 165, no. 8, Aug. 2018, doi: 10.1007/s00227-018-3385-0.

[17] R. E. Ball, M. K. Oliver, and A. B. Gill, "Early life sensory ability—ventilatory responses of thornback ray embryos (Raja clavata) to predator-type electric fields," *Dev. Neurobiol.*, vol. 76, no. 7, pp. 721–729, Jul. 2016, doi: 10.1002/dneu.22355.

[18] K. Formicki, A. Korzelecka-Orkisz, and A. Tański, "Magnetoreception in fish," *J. Fish Biol*., vol. 95, no. 1, pp. 73–91, Jul. 2019, doi: https://doi.org/10.1111/jfb.13998.

[19] M. M. Marcotte and C. G. Lowe, "Behavioral responses of two species of sharks to pulsed, direct current electrical fields: testing a potential shark deterrent," *Mar. Technol. Soc. J*., vol. 42, no. 2, pp. 53–61, 2008, doi: 10.4031/002533208786829133.

[20] B. Taormina et al., "Impact of magnetic fields generated by AC/DC submarine power cables on the behavior of juvenile European lobster (Homarus gammarus)," *Aquat. Toxicol*., vol. 220, Mar. 2020, doi: 10.1016/j.aquatox.2019.105401.

[21] Z. L. Hutchison, A. B. Gill, P. Sigray, H. He, and J. W. King, "A modelling evaluation of electromagnetic fields emitted by buried subsea power cables and encountered by marine animals: Considerations for marine renewable energy development," *Renew. Energy*, vol. 177, pp. 72–81, Nov. 2021, doi: https://doi.org/10.1016/j.renene.2021.05.041.

[22] A. B. Gill, Z. L. Hutchison, and M. Desender, "Electromagnetic Fields (EMFs) from subsea power cables in the natural marine environment". Cefas Project Report for Crown Estate Offshore Wind Evidence and Change Programme, 66 pp, 2023. [Online]. Available: https://tethys.pnnl.gov/sites/default/files/publications/Gill-et-al-2023-CEFAS.pdf

[23] M. Dhanak, E. An, R. Coulson, J. Frankenfield, S. Ravenna, D. Pugsley, G. Valdes, and W. Venezia., "AUV-based characterization of EMF emissions from submerged power cables," in *OCEANS 2015 - Genova*, Genova, Italy, 2015, pp. 1-6. doi: https://doi.org/10.1109/OCEANS-Genova.2015.7271719

[24] I. Donázar-Aramendía, M. J. Reyes-Martínez, C. Megina, M. Florido, and J. C. García-Gómez, "Assessing the effects of electromagnetic fields generated by submarine power cables on the soft-bottom community: An ecological in-situ study," *Environ. Res*., vol. 266, p. 120573, Feb. 2025, doi: 10.1016/j.envres.2024.120573.

[25] Z. L. Hutchison, A. B. Gill, P. Sigray, H. He, and J. W. King, "Anthropogenic electromagnetic fields (EMF) influence the behaviour of bottom-dwelling marine species," *Sci. Rep*., vol. 10, no. 1, Dec. 2020, doi: 10.1038/s41598-020-60793-x.

[26] R. Kavet, M. T. Wyman, and A. P. Klimley, "Modeling magnetic fields from a DC power cable buried beneath San Francisco Bay based on empirical measurements," *PLoS One*, vol. 11, no. 2, Feb. 2016, doi: 10.1371/journal.pone.0148543.

[27] J. Sherwood, S. Chidgey, P. Crockett, D. Gwyther, P. Ho, S. Stewart, D. Strong, B. Whitely, and A. Williams, "Installation and operational effects of a HVDC submarine cable in a continental shelf setting: Bass Strait, Australia," *J. Ocean Eng. Sci*., vol. 1, no. 4, pp. 337–353, Dec. 2016, doi: 10.1016/j.joes.2016.10.001.

[28] Z. Hutchison, P. Sigray, H. He, A. Gill, J King, C. Gibson, "Electromagnetic Field (EMF) Impacts on Elasmobranch (Shark, Rays, and Skates) and American Lobster Movement and Migration from Direct Current Cables," U.S. Department of the Interior, Bureau of Ocean Energy Management. OCS Study BOEM 2018-003., p. 254, Mar. 2018. [Online] Available: https://espis.boem.gov/final%20reports/5659.pdf

[29] P. Pettersson and N. Schonborg, "Reduction of power system magnetic field by configuration twist," *IEEE Trans. Power Deliv*., vol. 12, no. 4, pp. 1678–1683, 1997, doi: https://doi.org/10.1109/61.634190.

[30] G. D. Scott, M. A. Pooley, and B. R. T. Cotts, "Numerical and analytical modeling of electromagnetic fields from offshore power distribution cables," *IEEE Trans. Magn*., vol. 59, no. 5, May 2023, doi: 10.1109/TMAG.2023.3254885.

[31] C. Garrido, A. F. Otero, and J. Cidrás, "Low-frequency magnetic fields from electrical appliances and power lines," *IEEE Trans. Power Deliv*., vol. 18, no. 4, pp. 1310–1319, Oct. 2003, doi: http://dx.doi.org/10.1109/TPWRD.2003.817744.

[32] D. O. Carpenter and S. Ayrapetyan, "Exposure to and mechanisms of action of electric and magnetic fields," in *Biological effects of electric and magnetic fields: sources and mechanisms*, 1st ed., vol. 1, San Diego, California: Academic Press, 1994, ch. 1, pp. 21–21.